NASA Technical Paper 2739

August 1987

Evaluation of Installed Performance of a Wing-Tip-Mounted Pusher Turboprop on a Semispan Wing

James C. Patterson, Jr.,
and Glynn R. Bartlett

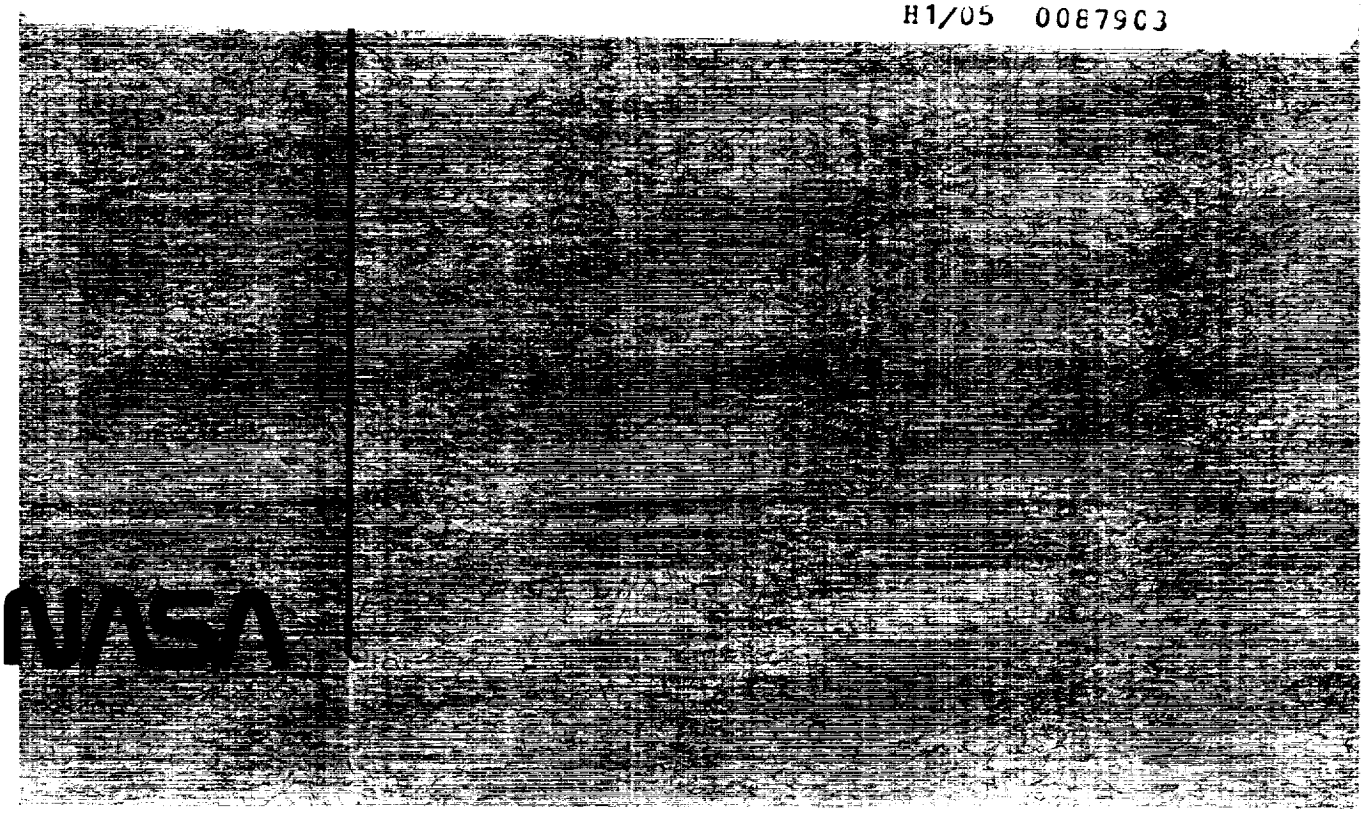

NASA Technical Paper 2739

1987

Evaluation of Installed Performance of a Wing-Tip-Mounted Pusher Turboprop on a Semispan Wing

James C. Patterson, Jr.,
and Glynn R. Bartlett

Langley Research Center
Hampton, Virginia

National Aeronautics
and Space Administration

Scientific and Technical Information Office

Summary

An exploratory investigation has been conducted at the Langley Research Center to determine the installed performance of a wing-tip-mounted pusher turboprop. Tests were conducted on a semispan model with an unswept, untapered wing and an air-driven motor that powered an SR-2 high-speed propeller located on the tip of the wing. All tests were conducted at a Mach number of 0.70 over an angle-of-attack range from approximately $-2°$ to $4°$ at a Reynolds number of 3.82×10^6 based on the wing reference chord of 13 in.

The data show that it is possible to improve propeller performance and simultaneously reduce the lift-induced drag of the wing. This improved performance is a result of locating the propeller behind the wing trailing edge at the wing tip in the crossflow of the wing-tip vortex.

Introduction

High-speed propeller designs have recently been developed that may be capable of obtaining the same thrust performance as present-day fan-jet engines while achieving a 15- to 20-percent fuel savings. These new propeller designs have generated considerable interest because of today's fuel economy consciousness. As a result, many research efforts are under way, in NASA and in industry, to optimize the propeller designs, to develop new turbine engines to drive the propellers, and to determine the installation effects of the turboprop on airplane performance. Both wind-tunnel and flight tests are being conducted.

As a result of these efforts, a number of turboprop/airframe integration concepts have been proposed. (See fig. 1.) The conventional tractor turboprop installation has several unfavorable characteristics. The propeller swirl and the increased velocities over the wing may have detrimental effects on the wing aerodynamics. This installation arrangement may also produce unfavorable noise effects on the fuselage and on the passengers. The other installation arrangements shown are attempts to overcome various problems associated with the conventional tractor installation (refs. 1 and 2). Research is being conducted on each of these concepts.

A turboprop installation location which has not been considered in any study to date is that of locating the turboprop on the wing tip. By locating the turboprop in a pusher fashion on the wing tip, such that the propeller is immersed in the lift-induced vortex flow behind the wing, it may be possible to take advantage of energy in the swirling vortex flow to enhance propeller performance as well as to disrupt the trailing vortex system by mass injection of the propeller wake into the vortex core. The exploratory research on this concept was conducted to quantify the potential benefits of mounting a pusher turboprop at the wing tip. However, the engine-out effect on the stability and control of the aircraft is a factor to be considered, but it is not addressed in this program. The directional control power of the double and triple slotted rudders now used on some transport type aircraft may be sufficient to control this effect.

This investigation was conducted in the Langley 7- by 10-Foot High-Speed Tunnel using a semispan model that had an unswept, untapered wing with a symmetrical airfoil section. (See fig. 2.) An air-driven turbine motor was used to drive a propeller mounted on the wing tip in a pusher position. The SR-2 propeller blade design discussed in reference 3 was used. All tests were conducted at a Mach number of 0.70, at angles of attack of approximately $-2°$ to $4°$, and at a Reynolds number of 3.82×10^6 based on the model wing chord of 13 in

Symbols

A_{cav}	cavity cross-sectional area between hub and nacelle, in^2
C_D	drag coefficient, $\frac{\text{Drag}}{q_\infty S}$
ΔC_D	engine installation drag coefficient, $C_{D,W/N} - C_{D,W}$
C_L	lift coefficient, $\frac{\text{Lift}}{q_\infty S}$
C_m	pitching-moment coefficient, referenced to wing quarter-chord, $\frac{\text{Pitching moment}}{q_\infty S \bar{c}}$
$\bar{c}$	mean geometric chord, in.
D_{main}	drag measured by main balance, lbf
F_N	propeller normal force
L	lift produced by propeller, lbf
N_i	nacelle incidence angle, deg
p_{cav}	cavity pressure between hub and nacelle, lbf/in^2
p_∞	free-stream static pressure, lbf/in^2
q_∞	free-stream dynamic pressure, lb/ft^2
S	exposed semispan wing area, 2.88 ft^2
S_{ext}	exposed semispan wing area including wing extension, 3.89 ft^2
T	thrust of propeller and hub, lbf

ΔT	thrust increase due to vortex flow field on propeller, lbf
T_{bal}	thrust measured by propeller balance, lbf
V_R	resultant velocity, ft/sec
V_∞	free-stream velocity, ft/sec
W	wing
W/N	wing/nacelle
α	angle of attack, deg
β	geometric pitch angle of propeller blade (referenced to propeller rotational plane), deg
θ_{prop}	angle of relative velocity due to propeller rotation, deg
ϕ_{vortex}	angle of relative velocity due to wing-tip vortex, deg

Design Philosophy

Propeller Performance Enhancement

The local velocity relative to a propeller blade is normally a combination of the rotational velocity of the propeller and that of the free stream. This is shown by a simple schematic in figure 3. The lift produced by each propeller blade is perpendicular to this local flow and is therefore not directed totally in a streamwise direction. A component of this lift in the flight-path direction is then the thrust produced by the propeller. A turboprop configuration installed in a pusher fashion at the wing tip experiences a change in the magnitude and direction of this relative velocity as a result of the addition of the lift-induced vortex flow that exists at the wing tip as shown in figure 3.

The increase in the angle between the relative velocity and the free stream should result in a more streamwise rotation of the propeller blade lift vector. Consequently, there is an increase in the propeller blade thrust component (fig. 3(b)). Therefore, a small reduction in blade pitch will be needed in the case of the full-scale aircraft to obtain a given thrust with the result that less engine power will be required.

Induced Drag Reduction

There are a number of other favorable effects that may result from the wing-tip pusher turboprop which tend to reduce the induced drag of the wing. The vortex flow shed from a lifting wing increases the wing downwash velocity normally produced by the wing in the process of developing lift. This downwash velocity increase, just behind the wing trailing edge, occurs without an additional increase in lift of the wing. In effect, this increase downwash velocity lowers the effective angle of attack of the wing and thus requires a physical increase in wing angle of attack to maintain the required lift. This change in angle of attack will result in induced drag (vortex drag). It was concluded in a study conducted on a semispan model with a turbofan nacelle located at the wing tip (refs. 4 and 5) that directing the high-energy mass wake of a jet engine into the vortex, which interrupts the core axial flow, dissipates the vortex. This interruption of the vortex flow resulted in a decrease in the downwash angle and, therefore, a significant decrease in the drag due to lift of the configuration. The propeller wake of the wing-tip-mounted pusher turboprop was expected to have a similar effect and produce a significant reduction in drag due to lift.

Apparatus and Experimental Methods

Test Facility

This investigation was conducted in the Langley 7- by 10-Foot High-Speed Wind Tunnel, which is a continuous-flow subsonic-transonic atmospheric wind tunnel. In the closed-test-section configuration, the speed range is from very low to approximately Mach 0.94, ending on model size. The test section is 6.584 ft high by 9.574 ft wide. The useable length of the test section is 10.833 ft with a mean cross-sectional area of 63.052 ft^2. The tunnel operates at ambient temperature and pressure and continuously exchanges air with the surrounding atmosphere for cooling. (See ref. 6.)

Model Configuration

Drawings of the semispan model used in this investigation are shown in figure 4. Figure 2 is a photograph of the model wall mounted in the wind tunnel with the wing-tip-mounted pusher turboprop installed.

The unswept, untapered wing shown in figure 4 has a chord of 13 in., an NACA 64_1A012 airfoil section, and an aspect ratio of 6.10 based on the full wing span of 79.26 in. The basic wing, wing plus wing-tip-mounted turboprop nacelle, and the wing turboprop nacelle plus wing extension configurations are shown in figure 4. The exposed basic wing area for the configuration under study was used as the reference area for the data obtained for the particular configuration (i.e., 2.88 ft^2 for the basic wing and 3.89 ft^2 for the wing with the tip extension).

High-pressure drive air powered the turboprop through a four-stage air turbine motor connected to the propeller through a shaft system (fig. 4(b)). The air turbine motor was mounted on the wing inside the fuselage, so not to affect the main balance forces or the aerodynamic forces. The power output shaft extended along and inside of the wing leading edge from the engine location to the wing tip. Power was then transferred to the propeller shaft through a set of 90° helical bevel gears. The drive air was exhausted into the inner section of a dual annular exhaust system after passing through the air turbine motor. This inner annular section carried the expanded cold exhaust air of the turbine motor, which then was exhausted into the tunnel plenum chamber. Because of the proximity of the exhaust to the model's main force balance, the outer annular section carried a low flow rate of warm air from the heated drive air supply to insulate the model balance from the cold exhaust, as shown in figure 4(b). The exhaust flow was aligned with the center of the model main balance in the side-force direction. Since the balance does not measure side force, the force term caused by the exhaust flow was eliminated from the balance measurements.

Force Balances

Measurements of forces and moments were obtained by an internally mounted, wall-supported, five-component, electrical strain-gage balance. The model was designed so that the wing attached directly to the balance and protruded through a clearance opening in the nonmetric fuselage. The fuselage (actually a balance fairing), attached to the wind-tunnel wall but not to the balance, was designed to traverse the angle-of-attack range without the fuselage forces being measured by the balance.

The main model balance measures the drag of the complete model minus the thrust from the turboprop. To determine the actual drag of the complete model, the thrust of the turboprop must be added to the main balance drag measurements. To obtain these data, a three-component internal electrical strain-gage thrust balance capable of measuring propeller thrust, propeller lift, and pitching moment was installed in the aft end of the turboprop nacelle. (See fig. 4(b).) The propeller was attached directly to the balance shaft while the other end of this balance was driven, through a flex coupling, by the turbine air motor. The balance housing was fixed to the nacelle, but the balance shaft and bearings held by the balance beams were free to move under the influence of the forces produced by the propeller. The propeller balance allows a direct measurement of the propeller performance and thrust to be used in combination with the main balance. A detailed description of the measured forces and bookkeeping system is given in the appendix.

The thrust component in the lift direction was small, even at the highest angle of attack tested, compared with the lift of the wing. Therefore, the lift-coefficient values presented have not been corrected for the effect of propeller thrust.

Drive Air System

The drive air system consists of a high-pressure air supply, an air turbine motor, and an exhaust system. The high-pressure drive air was controlled by two valves upstream of the motor. One valve was used to set the maximum pressure in the system, and the other valve controlled the air turbine drive pressure. By changing the air turbine drive pressure, it was possible to vary the thrust output of the propeller. A pop-off valve was located between the control valve and the turbine motor to prevent a possible overpressure. Upstream of the control valves was a steam heater to control drive air temperature to the air turbine motor.

Turboprop Turbine Horsepower

Measurements of the airflow were made to facilitate calculation of power output of the air turbine motor. A critical venturi installed between the two control valves measured mass flow rate through the air turbine motor. Both pressure and temperature were measured upstream and downstream of the air turbine motor to determine the pressure drop and change in temperature. A magnetic pickup measured the revolutions per minute of the air turbine motor. The horsepower output of the air turbine motor was calibrated dependent on mass flow, inlet pressure, and rpm. These calibration curves were then used to determine the power output of the turbine for the different test conditions.

Tests

All tests were conducted at a Mach number of 0.70 over an angle-of-attack range from $-2°$ to $4°$ at a tunnel total pressure of 2120 lb/ft^2 and a total temperature of 120°F. These conditions resulted in a Reynolds number of 3.82×10^6 based on the mean wing chord.

Boundary-layer transition strips, 0.125 in. wide, consisting of No. 120 carborundum grains, were installed on the upper and lower surfaces of the wing 0.7 in. behind the wing leading edge. The location of fully turbulent flow was thus established.

The wing fuselage was tested as a baseline configuration with a symmetrical fairing on the wing tip (wing-tip cap). The wing-tip-mounted pusher turboprop was tested at a constant-thrust output level

from the propeller throughout the angle-of-attack range at two nacelle incidence angles of 0° and −3°. This was followed by tests conducted with a 9-in. wing extension attached to the outer surface of the wing-tip-mounted nacelle. (See fig. 4(a).)

Results

Propeller Performance

The interaction of the lift-induced vortex with the wing-tip-mounted pusher turboprop resulted in a thrust enhancement that may be seen in figure 5. The power required for cruise conditions at $C_L = 0$, where no vortex exists, has been nondimensionalized and is presented against lift coefficient. As the lift coefficient of the wing was increased, a vortex flow was created which changed the incoming flow angle to the propeller. As a result, at a lift coefficient of 0.3, the power required to maintain the same zero-lift thrust value was reduced by approximately 13 percent. This result is probably caused by an increase in propeller effective pitch angle caused by the vortex cross flow. In the case of the full-scale aircraft, the propeller-blade pitch angle is variable, which allows the pitch to be reduced; therefore, the rpm may be held constant, which results in a lower fuel rate to the engines.

To simulate the pusher turboprop located other than at the wing tip, tests were conducted with a 9-in. wing extension attached to the outboard surface of the nacelle. There was approximately a 10-percent increase in power required at $C_L = 0$ compared with that of the wing-tip-mounted, turboprop configuration. This may be the result of the propeller being located totally behind the wing where the wing wake effects, including the interference associated with two wing nacelle junctures, reduce the propeller performance. There was a negligible reduction in power required for constant thrust with increasing lift coefficient. This would indicate a lack of vortex thrust enhancement such as that obtained by the pusher turboprop located at the wing tip. With the tip extension installed, the wing-tip vortex was transferred from the propeller location to the new wing tip, and the favorable thrust effect resulting from the vortex/propeller interaction no longer existed.

Drag-Coefficient Characteristics

The aerodynamic effect on drag resulting from mounting a high-performance pusher turboprop/nacelle on the wing tip of the basic wing is presented in figure 6. Adding the unpowered nacelle to the wing results in the expected drag increase at zero lift. This increment is primarily the result of the added skin-friction drag of the nacelle (estimated to be about 0.0016). As the lift coefficient increases, the drag increment caused by the nacelle also increases. This added drag is probably caused by the interference in the juncture between the nacelle and wing under lifting conditions and by the increase in nacelle form drag.

Adding power at either blade rotation angle results in a significant decrease in drag due to lift in the normal operating range. At a lift coefficient of approximately 0.40, the power effect causes a reduction in drag equal to the addition of the nacelle. This effect is discussed in more detail in the section "Induced Drag Characteristics."

A nacelle incidence angle of −3° was employed in an attempt to increase the effectiveness of the turboprop/vortex interaction by placing the propeller above the wing chord plane where it could be more aligned with the vortex flow. The vortex tends to form just above the wing trailing edge before moving downward under the influence of the downwash of the wing. The resulting drag-coefficient characteristics for this configuration are presented in figure 7. Adding power to the nacelle at either blade angle significantly reduces the drag due to lift; at lift coefficients above about 0.1, drag values lower than the value for the wing alone are obtained. Evidently, this more favorable location of the propeller wake system has a more pronounced effect on the vortex and the wing downwash system than does the propeller wake for the nacelle at zero incidence, which reduces the drag approximately 10 percent. (See figs. 6 and 7.)

To determine the effect on drag of a pusher turboprop located other than at the wing tip, a 9-in. wing section was added outboard of the nacelle as stated previously (see fig. 4), and the results are presented in figure 8. The installed drag associated with the unpowered nacelle is more than twice that of the wing-tip-mounted nacelle (figs. 6 and 8); this result should be expected with a wing-nacelle juncture on both sides of the nacelle. There is a favorable effect of propeller thrust on this large interference drag; the lower propeller pitch angle ($\beta = 55.1°$) is more effective. There is probably an entrainment of flow in the region of the wing/nacelle juncture that is caused by the turboprop high-speed wake. This wake reduces or eliminates some of the adverse flow effects, which results in a reduction in the drag. The configuration with the nacelle at −3° has a lower drag due to lift than the configuration with the 9-in. wing-tip extension. (Compare fig. 8 with the wing configuration of fig. 7.) The data indicate that disrupting the wing-tip vortex by the wake from the turboprop may be a more effective way of reducing the drag due to lift than extending the wing tip.

Lift-Coefficient Characteristics

The variations in lift coefficient with angle of attack for the wing, wing/nacelle, and wing/nacelle/propeller configurations are presented in figure 9. An increase in lift at a fixed angle of attack is indicative of a reduction in the lift-induced drag. This increase in lift would result from a reduction in the effect of the lift-induced vortex on the wing downwash field, which increases the effective angle of attack of the wing. The addition of the unpowered nacelle to the wing tip results in an increase in the lift-curve slope of the configuration. This increase is probably the result of the "end plate" effect resulting from the physical presence of the nacelle at the wing tip, the wing now being nonplanar. The data also indicate that there is a further increase in lift-curve slope as a result of the addition of power. This increase is probably due to the vortex attenuation effect derived from the propeller wake/vortex interaction, which results in a further increase in effective angle of attack of the wing.

Changing the nacelle incidence angle by $-3°$ results in a shift in the angle of attack for zero lift with essentially no change in the lift-curve slope. (See fig. 10.) This result was expected because of the size the nacelle that was deflected $-3°$. The results with power are essentially the same as those noted for the undeflected nacelle. (See fig. 9.) Therefore, the mechanism for the drag reduction and lift changes noted should be the same.

The results of the addition of the wing-tip extension on the basic data of the wing/nacelle/propeller configuration with a $0°$ angle of incidence are presented in figure 11. With the nacelle installed, other than at the wing tip, there is a minimal increase in slope of the lift curve. The effect of installing the nacelle/propeller inboard of the wing tip, out of the vortex flow, greatly reduced its favorable effect on the wing.

Pitching-Moment-Coefficient Characteristics

The pitching-moment coefficient is presented against lift coefficient in figure 12. The installation of the unpowered nacelle at the wing tip at $0°$ nacelle incidence (fig. 12(a)) did not change the static margin of the wing alone but did shift the zero-lift pitching-moment coefficient in a positive direction. Adding power to the configuration with either nacelle incidence ($0°$ or $-3°$) resulted in a stable shift in the static stability level. This stable effect is maintained throughout the lift range and is probably a result of the changes in loading on the wing, which is caused by the propeller wake effects on the wing downwash.

Pitching-moment results for $0°$ nacelle incidence with wing-tip extension are presented in figure 12(c). The nacelle-alone installation causes a slight reduction in the static stability level, which is offset by the propeller effects and is equal to the wing-alone results.

Induced Drag Characteristics

A comparison of the change in drag between the basic wing and each wing-tip-mounted pusher turboprop configuration is presented in figure 13 at a lift coefficient of 0.3.

The installed drag of the nacelle mounted on the wing tip of the basic wing, without propeller, is approximately eight counts greater than the calculated flat-plate skin-friction drag based on the wetted area of the nacelle (dashed line in fig. 13). This difference includes form drag and possibly some interference drag of the wing/nacelle combination. The installed drag increment of the nacelle-turboprop configuration with a blade pitch angle of $57°$ is approximately one-fifth of that of the wing-nacelle configuration. This drag reduction is probably due mainly to an induced drag reduction of the wing associated with the turboprop/vortex interaction (refs. 7 and 8). The vortex flow may be altered by the interruption of the vortex core axial flow by the propeller wake. This interruption causes the vortex to dissipate and thereby reduce its effect on the wing downwash field resulting in a reduction in induced drag.

Although the lower pitched blades have higher drag at $C_L = 0$ (fig. 6), possibly because of the greater propeller frontal area, they are more effective in reducing induced drag over the lift range above $C_L = 0.2$. At the highest test lift coefficient, the drag due to lift of the wing for the lower pitched blades is greater than that for the high pitched blades due possibly to the degree of propeller/vortex-flow interaction.

In an attempt to further reduce the drag of the wing/nacelle combination, the nacelle was set at $-3°$ incidence relative to the wing as stated previously. (See fig. 13(a).) When the wing is set near the cruise angle of attack of $3°$, the nacelle is near $0°$ angle of attack relative to the flight path, which should contribute to the overall reduction in drag due to the reduced nacelle frontal area. The turboprop wake is nearer the center of the vortex at this incidence angle, and its effect on induced drag is shown by the bar graph in figure 13(a). The negative nacelle incidence resulted in an additional reduction in drag at lift coefficients of 0.3, such that the drag is less than that of the basic wing. The basic wing results do not include any nacelle drag. Again, the lower

propeller pitch angle is more efficient, as in the case of the zero incidence.

Direction of Propeller Rotation

The effect of rotating the turboprop in the same direction as the wing-tip vortex (prorotation, C_D in the negative C_L range shown in figs. 5 and 6) instead of in a counterrotational direction is presented in figure 13(b). There is a drag increase associated with the prorotation case, as would be expected. This increase is due to a reduction in the relative propeller blade pitch angle, which requires a higher rpm (ref. 9) and a higher power input to the turbine in the negative lift range (fig. 5) to maintain the constant thrust level used in this investigation.

There was no induced drag reduction with the tip extension installed (0° incidence) as can be seen in the bar chart in figure 13(c). When the tip vortex was moved away from the propeller plane, the induced drag reduction was lost.

Increased Lift Coefficient

A comparison of the change in drag between the basic wing and wing-tip-mounted pusher turboprop is presented at a lift coefficient of 0.4 in figure 14. Trends at $C_L = 0.4$ are similar to those at $C_L = 0.3$, and the favorable effect of the interaction of the wing-tip-mounted pusher turboprop and the vortex at the higher lift coefficient is probably due to the increased strength of the wing-tip vortex associated with the higher lift coefficient (fig. 14(a)). An increased installed drag for the extended wing/nacelle at $C_L = 0.4$ is presented in figure 14(b) compared with that at $C_L = 0.3$ in figure 13(c). This increase is probably the result of the increase in wing/nacelle interference at this greater lift coefficient.

Conclusions

An exploratory investigation has been conducted at the Langley Research Center to determine the installed performance of a wing-tip-mounted pusher turboprop. The study utilized a semispan model that had an unswept, untapered wing with a symmetrical airfoil section and an air-driven motor to power an SR-2 high-speed pusher propeller located on the tip of the wing. The results of this study indicated the following:

1. The performance of a propeller located just behind the wing tip is increased as a result of the influence of the wing-tip vortex flow.

2. The effect of the propeller wake on the wing-tip vortex resulted in a reduction in the drag due to lift of the wing at each nacelle incidence tested.

3. The propeller performance enhancement and the reduction in drag due to lift associated with the wing-tip pusher turboprop is forfeited when the turboprop is located inboard of the wing tip (wing tip extended).

4. A $-3°$ turboprop nacelle incidence resulted in an additional drag reduction of approximately 10 percent at a lift coefficient of 0.3.

NASA Langley Research Center
Hampton, VA 23665-5225
June 29, 1987

Appendix

Measured-Forces Bookkeeping

Forces

The force measurements of the balance have been reduced to coefficient form using the exposed semispan wing area.

Thrust

The thrust of the propeller and hub was obtained from the thrust balance minus the pressure force between the hub and nacelle as follows:

$$T = T_{\text{bal}} - A_{\text{cav}} \, (p_{\text{cav}} - p_{\infty})$$

Drag

The drag of the model was obtained from the measurements of the main balance, located inside the fuselage, plus the thrust balance measurements, located in the nacelle. The sum of these measurements are the total drag of the wing/nacelle configuration as follows:

$$\text{Drag} = D_{\text{main}} + T$$

The model coefficients were then determined by dividing the forces by the dynamic pressure and exposed wing area as follows:

$$C_D = \frac{\text{Drag}}{q_\infty S}$$

$$C_L = \frac{\text{Lift}}{q_\infty S}$$

$$C_m = \frac{\text{Pitching moment}}{q_\infty S \bar{c}}$$

References

1. Abeyounis, William K.; and Patterson, James C., Jr.: *Effect of Underwing Aft-Mounted Nacelles on the Longitudinal Aerodynamic Characteristics of a High-Wing Transport Airplane.* NASA TP-2447, 1985.
2. Lamb, Milton; Abeyounis, William K.; and Patterson, James C., Jr.: *Nacelle/Pylon/Wing Integration on a Transport Model With a Natural Laminar Flow Nacelle.* NASA TP-2439, 1985.
3. Stefko, George L.; and Jeracki, Robert J.: *Wind-Tunnel Results of Advanced High Speed Propellers in the Take-off, Climb, and Landing Operation Regimes.* NASA TM-87054, 1985. (Available as AIAA-85-1259.)
4. Patterson, James C., Jr.; and Flechner, Stuart G.: *An Exploratory Wind-Tunnel Investigation of the Wake Effect of a Panel Tip-Mounted Fan-Jet Engine on the Lift-Induced Vortex.* NASA TN D-5729, 1970.
5. Patterson, James C., Jr.; and Jordan, Frank L., Jr.: *Thrust-Augmented Vortex Attenuation. Wake Vortex Minimization,* NASA SP-409, 1977, pp. 251-270.
6. Fox, Charles H., Jr.; and Huffman, Jarrett K.: *Calibration and Test Capabilities of the Langley 7- by 10-Foot High Speed Tunnel.* NASA TM X-74027, 1977.
7. Patterson, James C., Jr.; and Flechner, Stuart G.: *Exploratory Wind-Tunnel Investigation of a Wingtip-Mounted Vortex Turbine for Vortex Energy Recovery.* NASA TP-2468, 1985.
8. Patterson, James C., Jr.: Vortex Attenuation Obtained in the Langley Vortex Research Facility. *J. Aircr.,* vol. 12, no. 9, Sept. 1975, pp. 745–749.
9. Patterson, James C., Jr.; and Bartlett, Glynn R.: Effect of a Wing-Tip Mounted Pusher Turboprop on the Aerodynamic Characteristics of a Semi-Span Wing. AIAA-85-1286, July 1985.

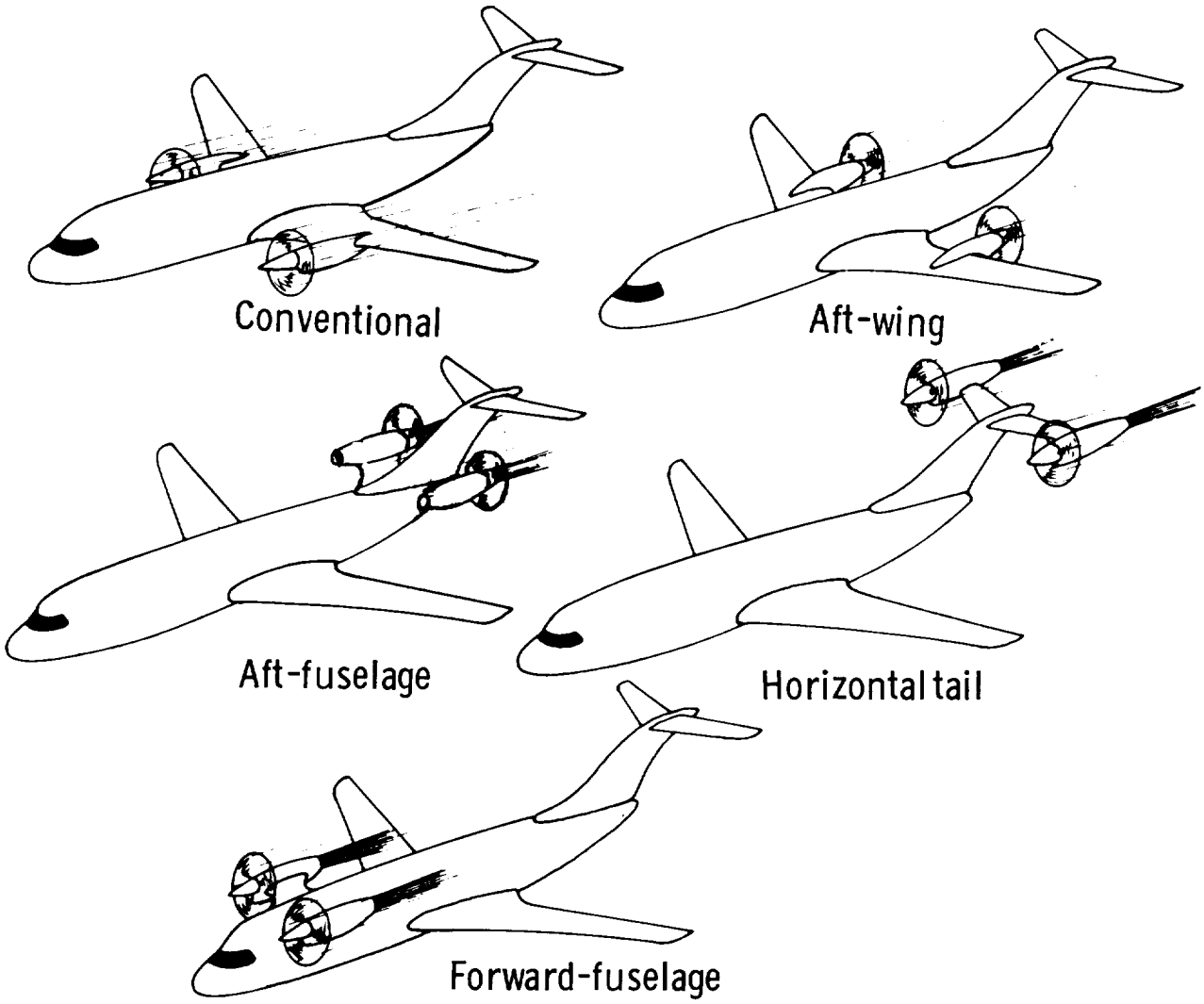

Figure 1. Possible types of turboprop installations.

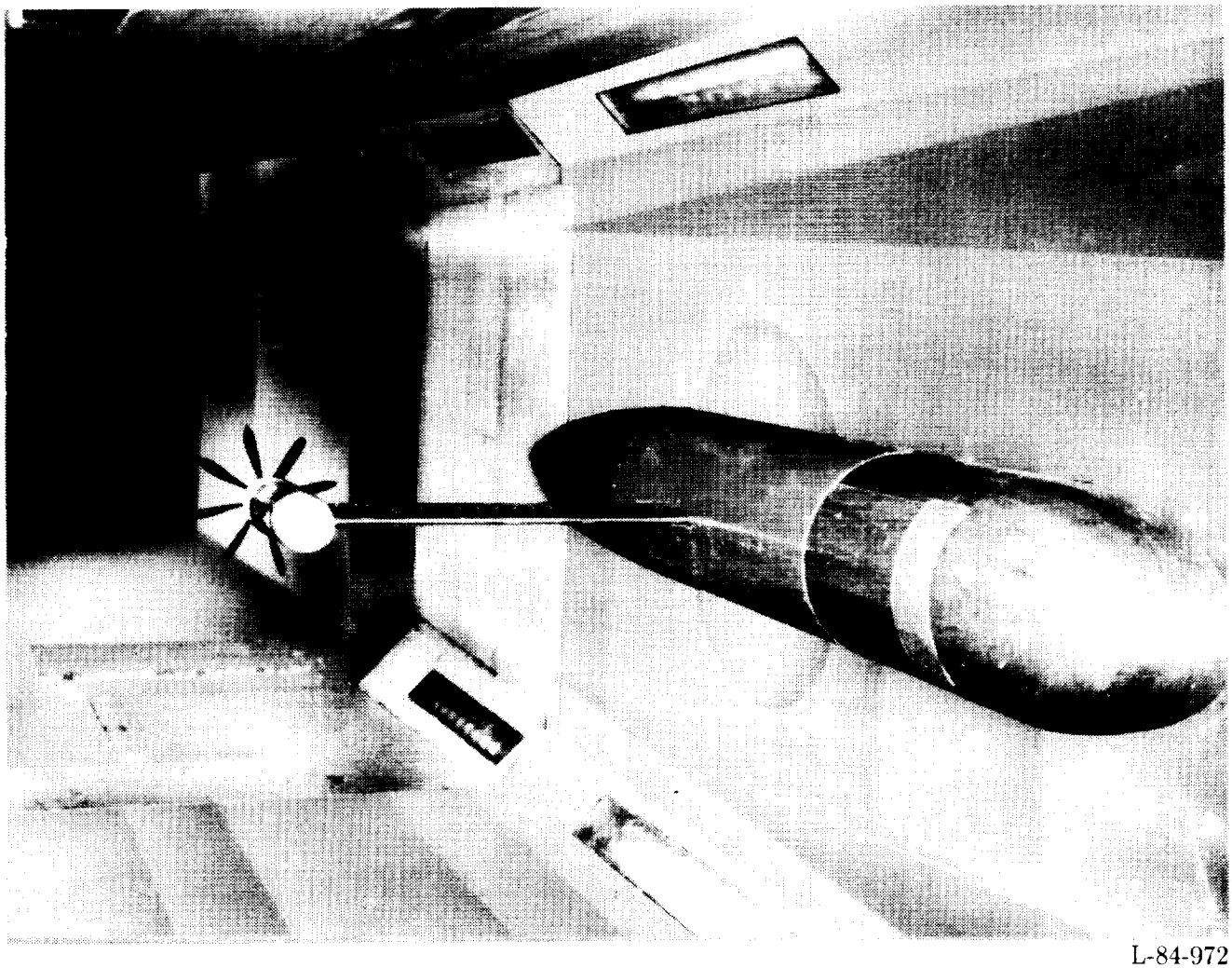

L-84-972

Figure 2. Wing-tip-mounted pusher turboprop model in Langley 7- by 10-Foot Speed Tunnel.

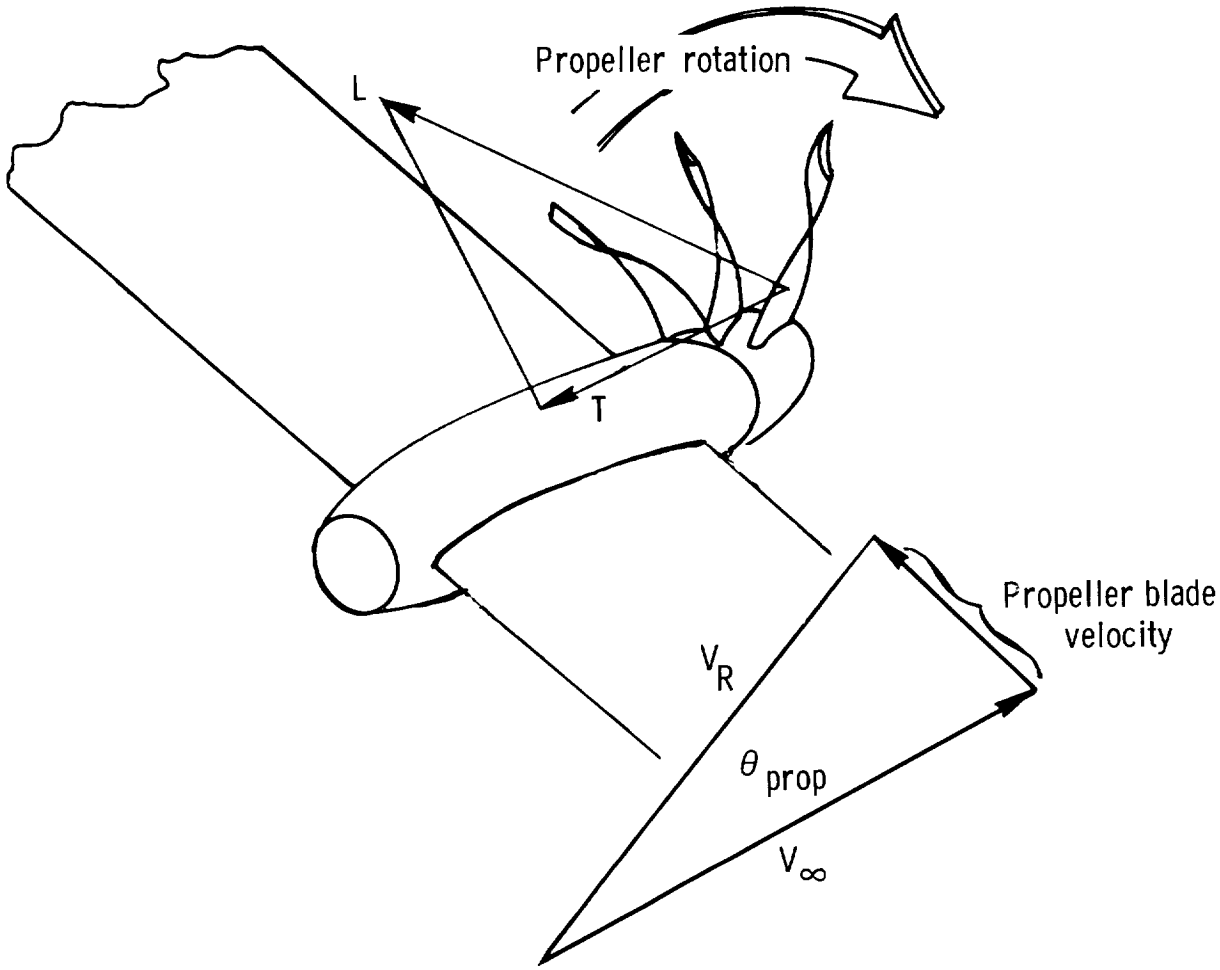

(a) Normal velocity components on propeller blade.

Figure 3. Vortex enhancement of propeller efficiency.

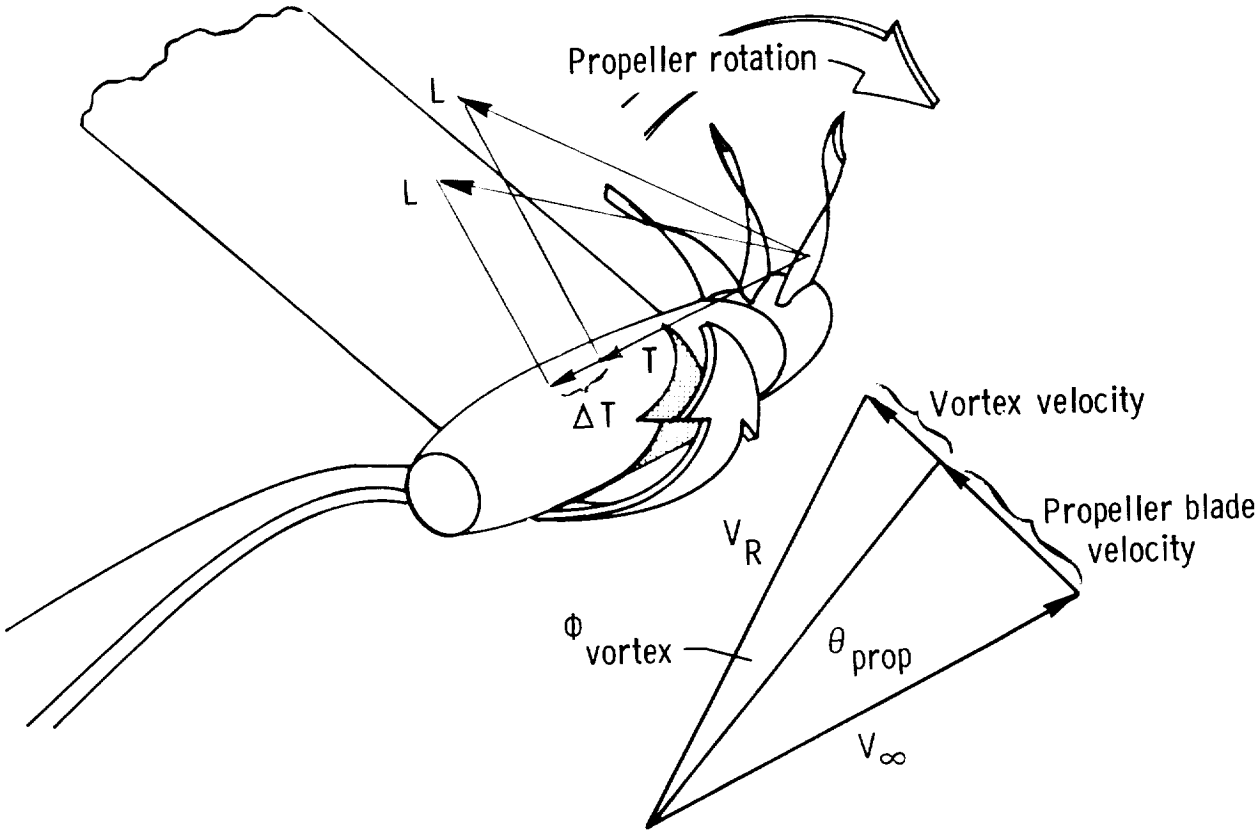

(b) Change in velocity components due to vortex flow.

Figure 3. Concluded.

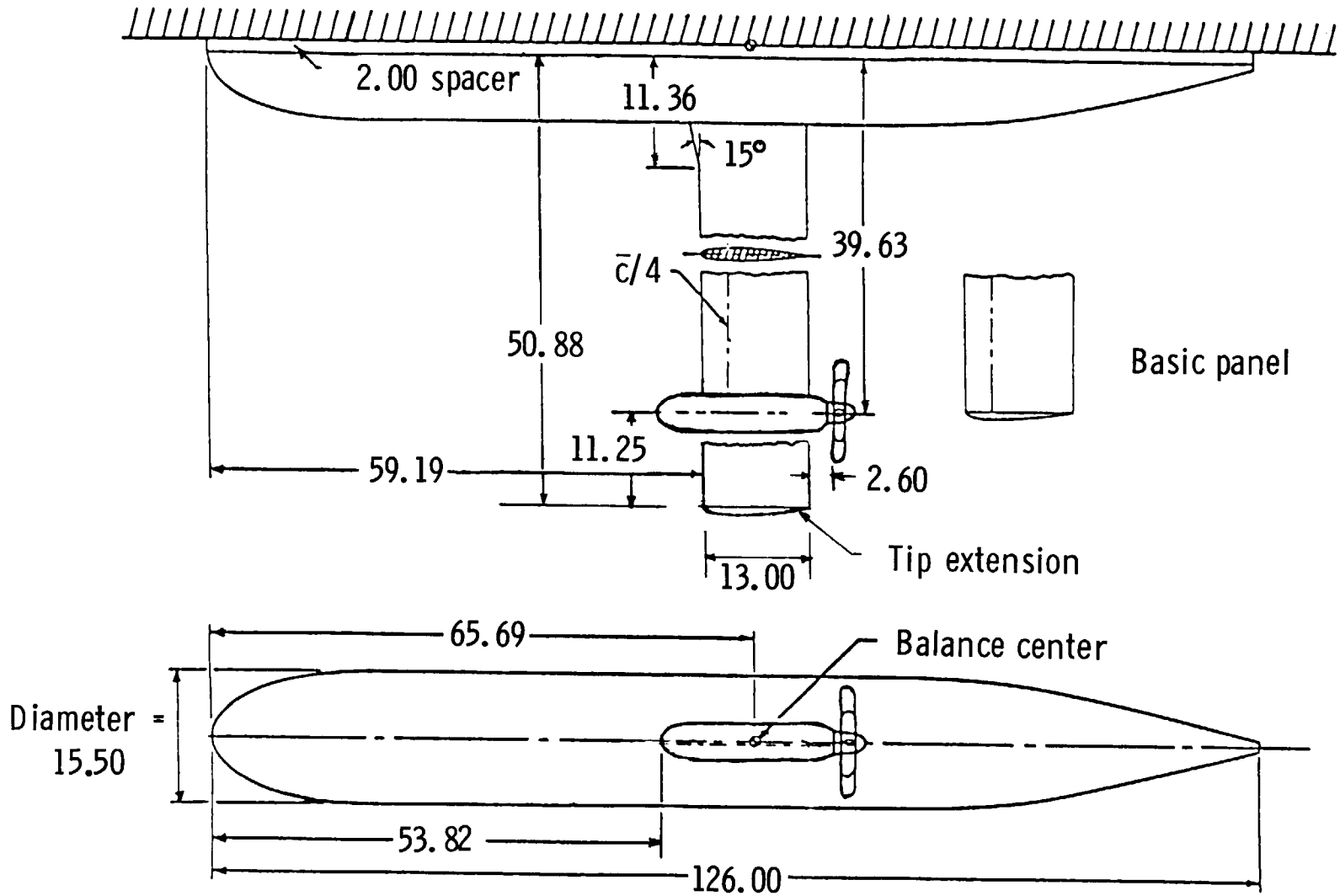

(a) Schematic of wing, fuselage, and pusher turboprop.

Figure 4. Drawings of semispan model. Dimensions are in inches unless otherwise noted.

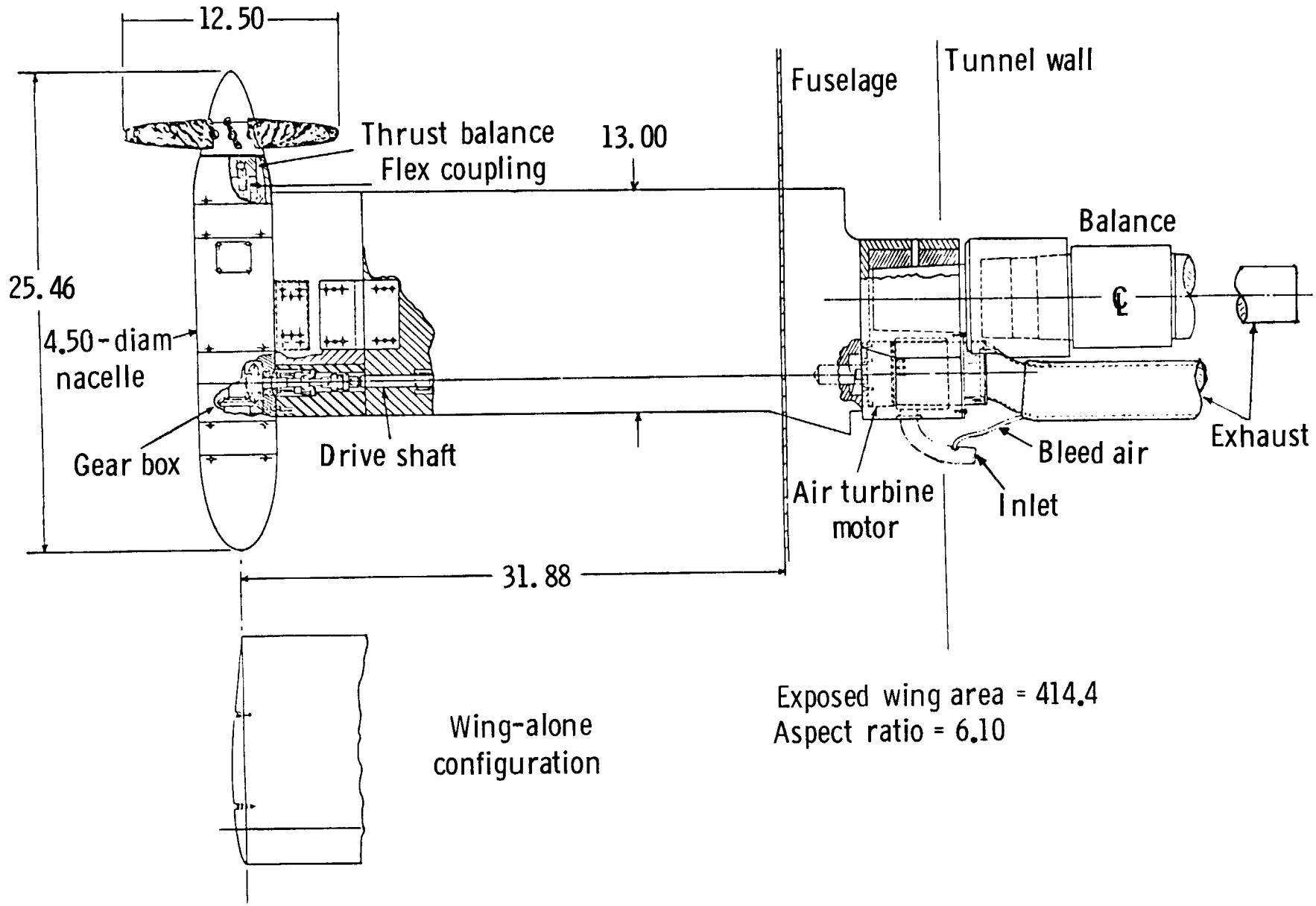

(b) Details of main and turboprop balances and turbine drive system.

Figure 4. Concluded.

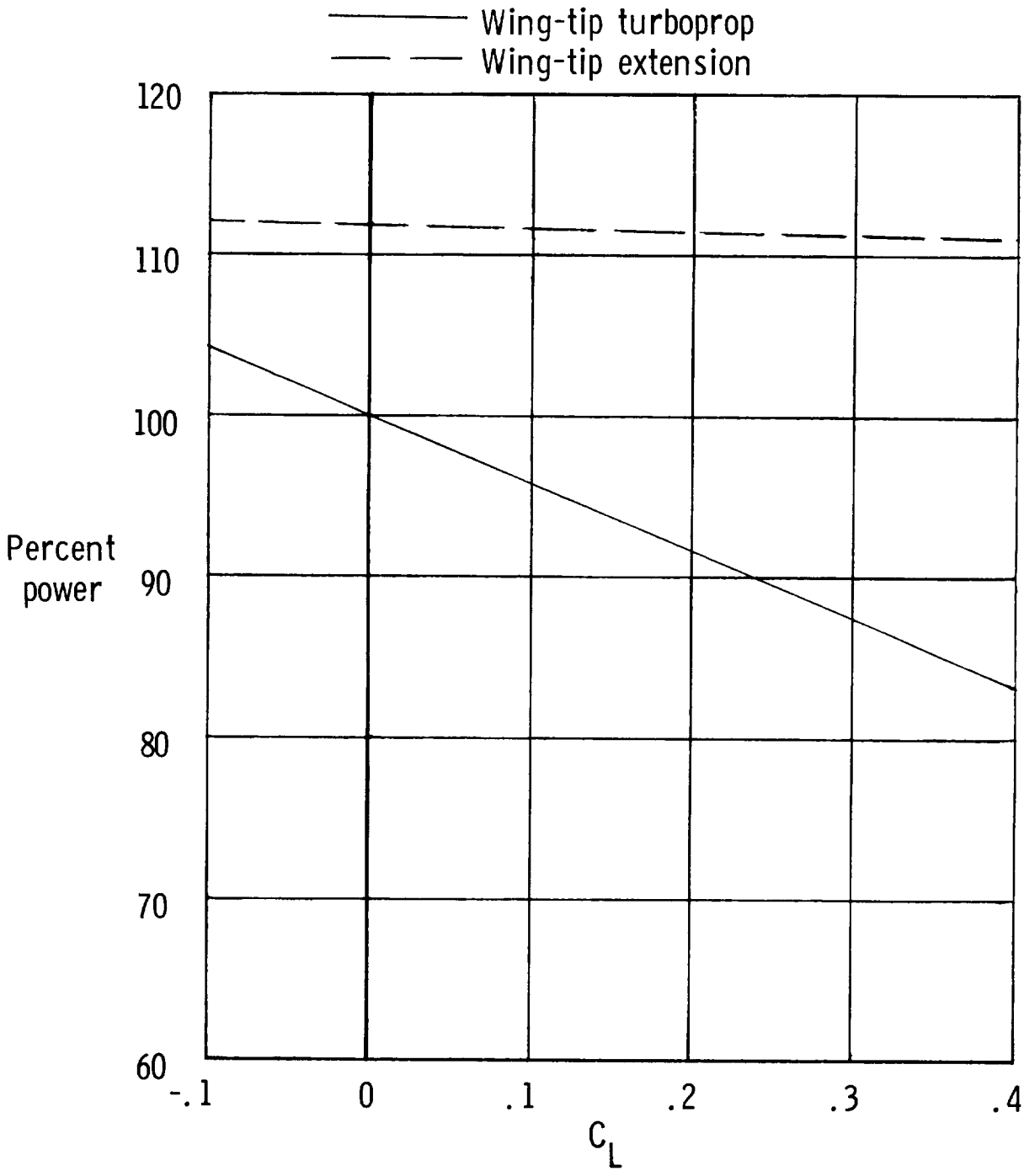

Figure 5. Propeller power requirements for constant thrust at 0° incidence.

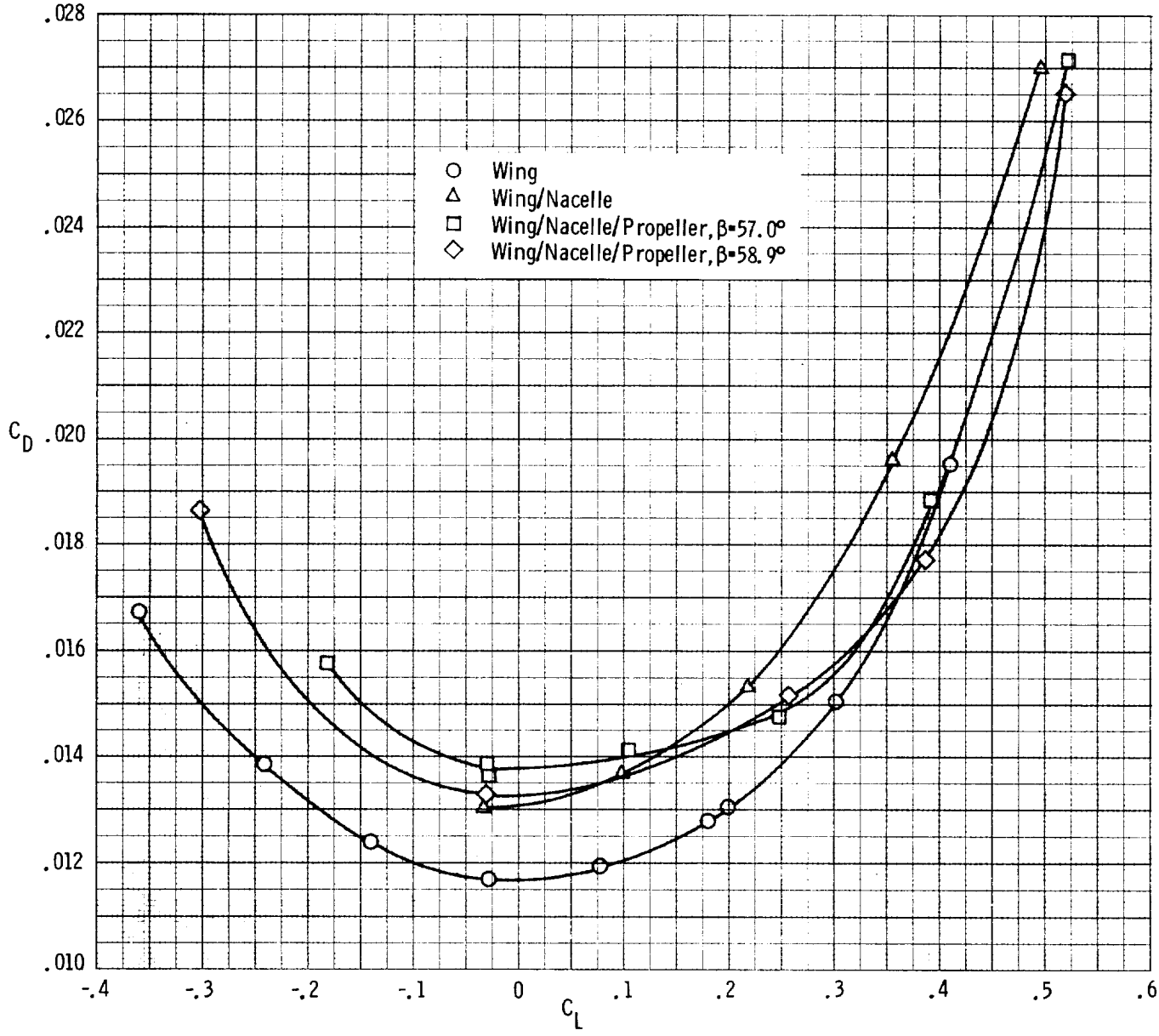

Figure 6. Vortex/propeller interaction on drag coefficient versus lift coefficient for 0° incidence.

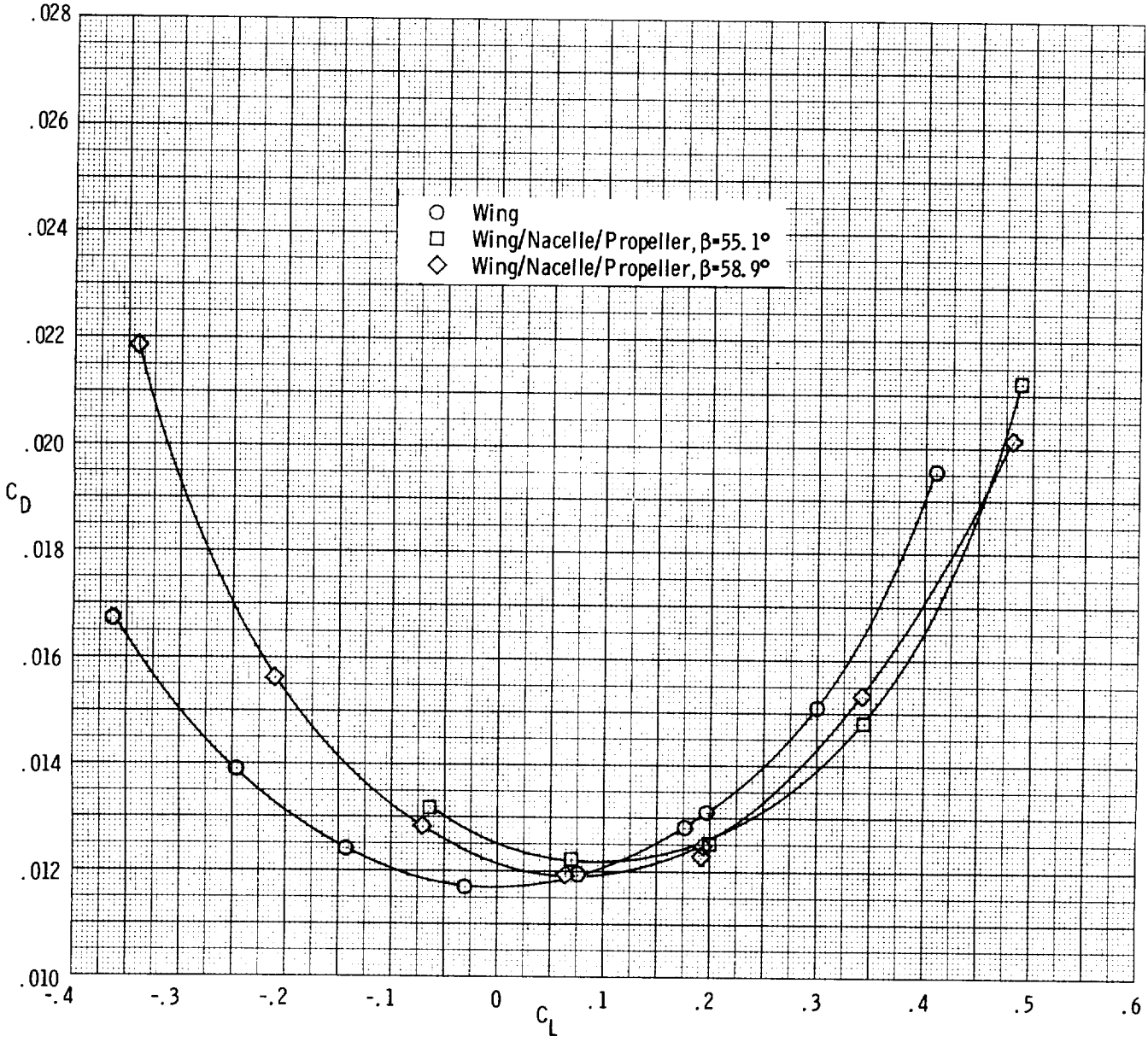

Figure 7. Vortex/propeller interaction on drag coefficient versus lift coefficient for −3° incidence.

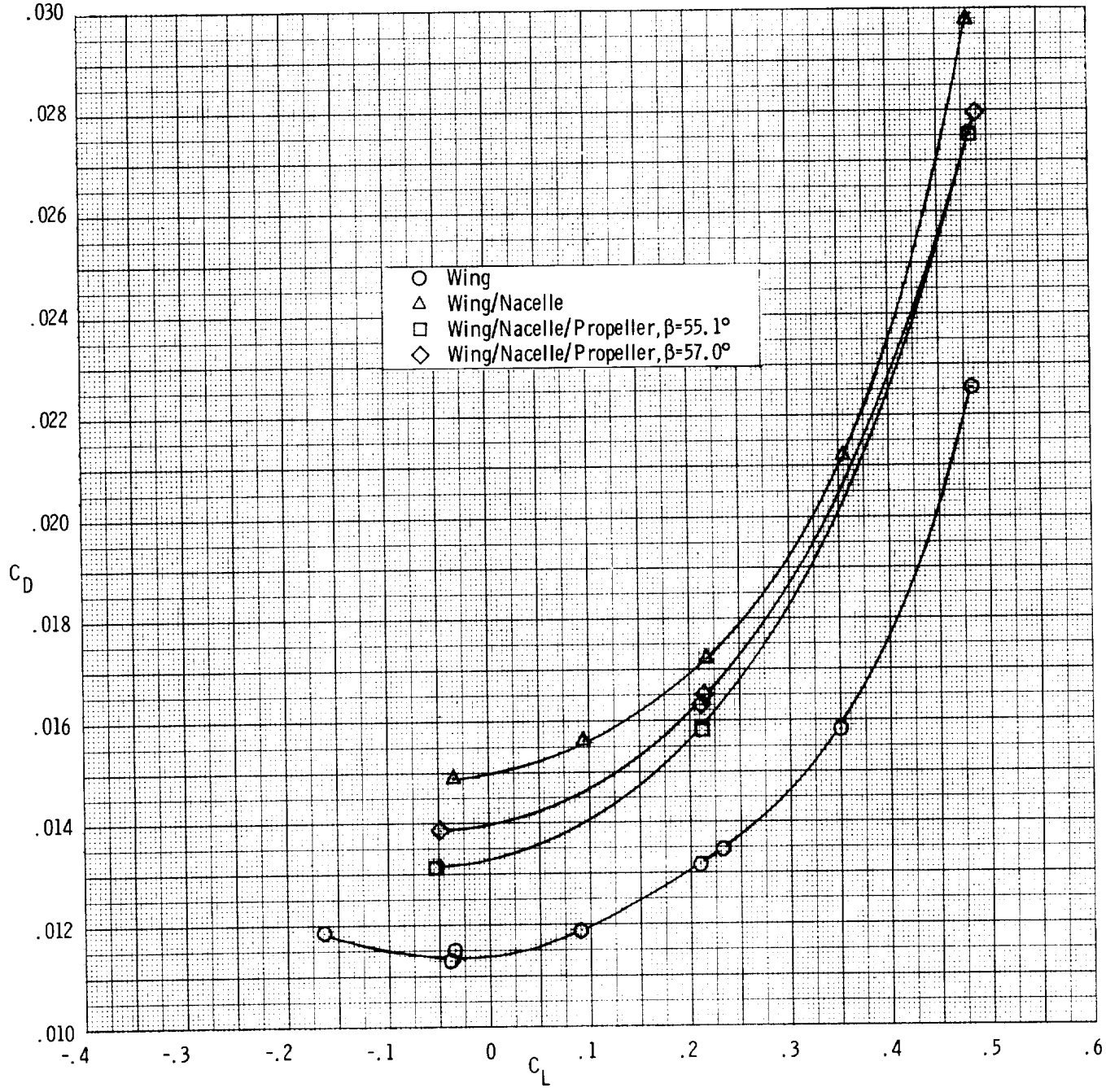

Figure 8. Vortex/propeller interaction on drag coefficient versus lift coefficient for 0° incidence with wing-tip extension.

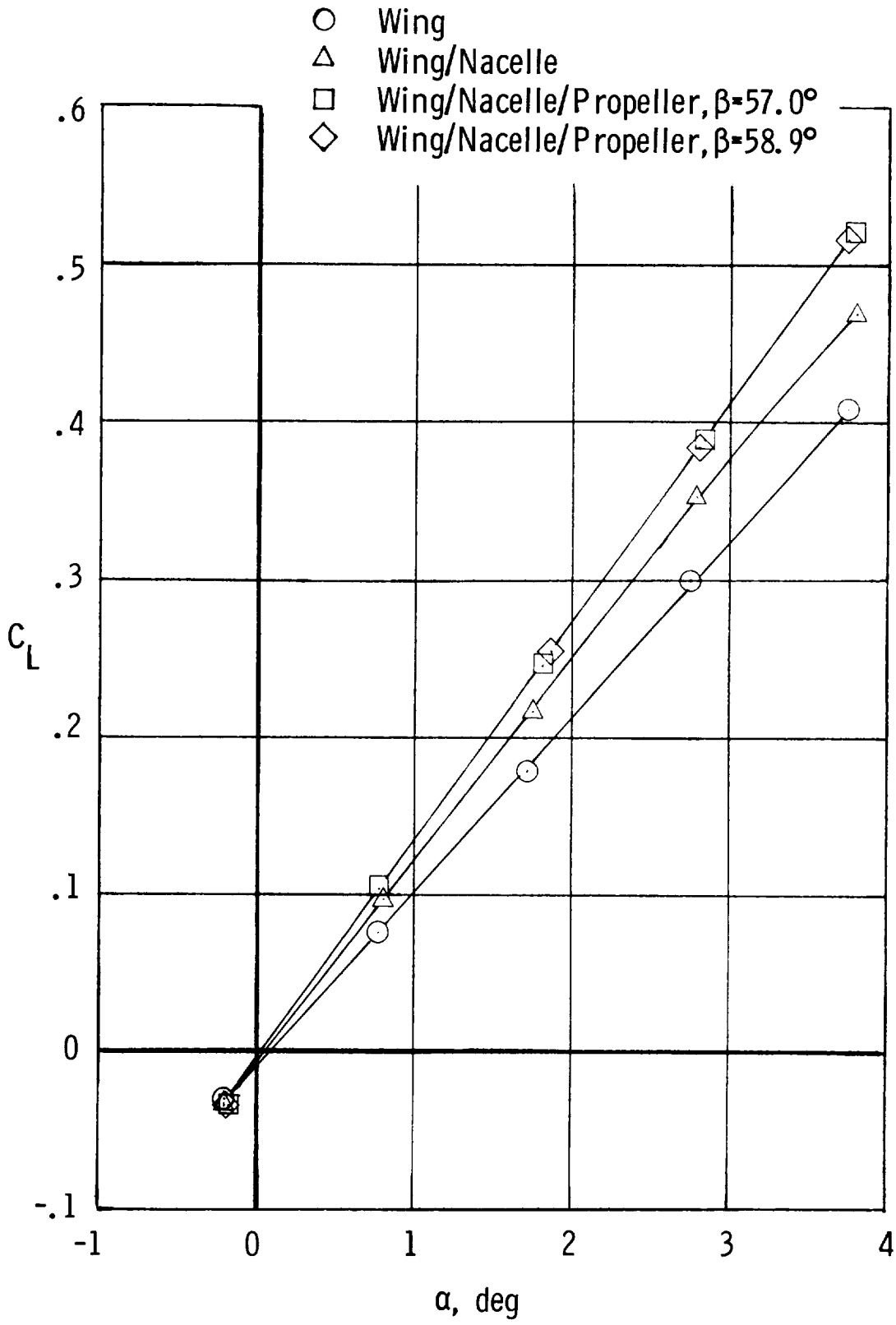

Figure 9. Effect of nacelle and propeller installation on lift coefficient versus angle of attack at 0° incidence.

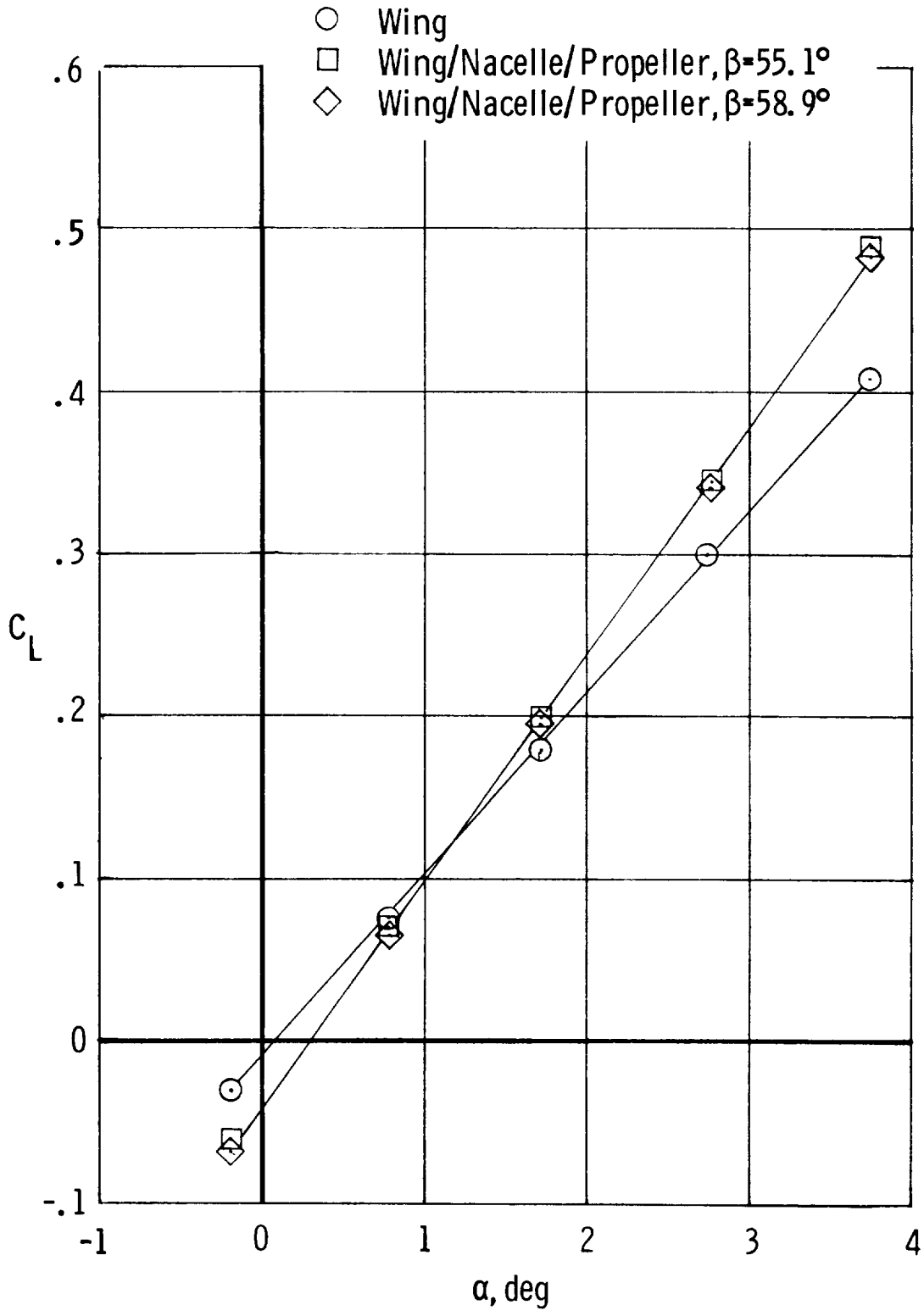

Figure 10. Effect of propeller installation on lift coefficient versus angle of attack at −3° incidence.

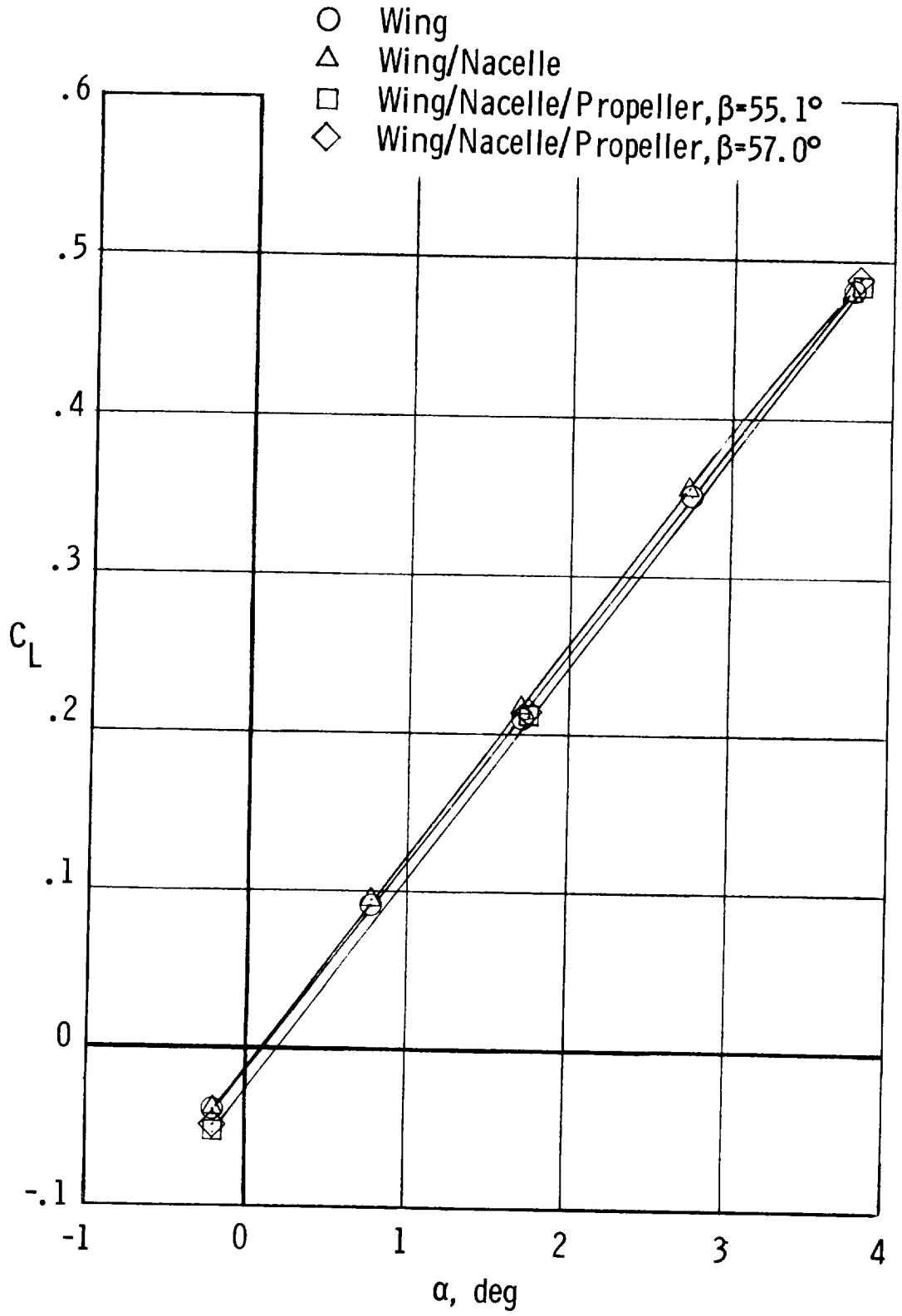

Figure 11. Effect of nacelle and propeller installation on lift coefficient versus angle of attack at 0° incidence with wing-tip extension.

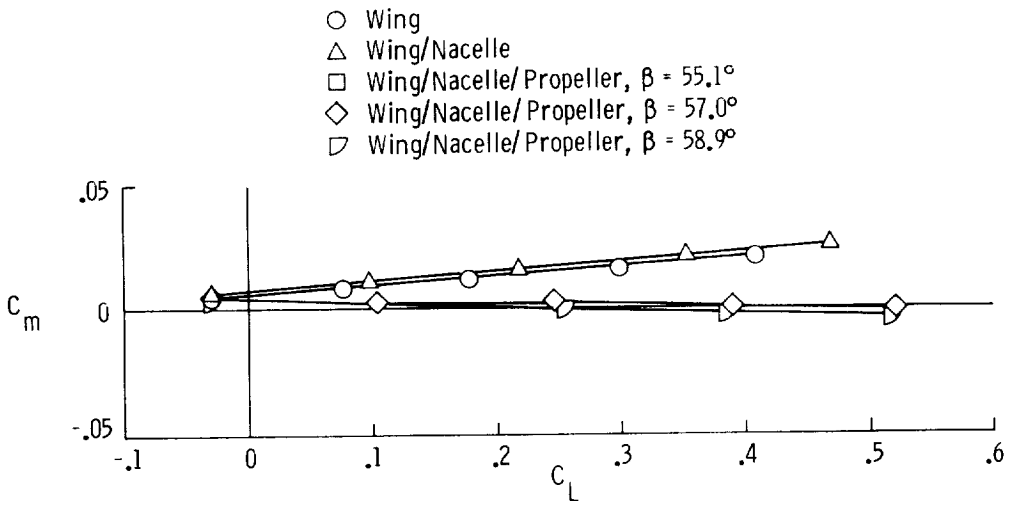

(a) 0° nacelle incidence.

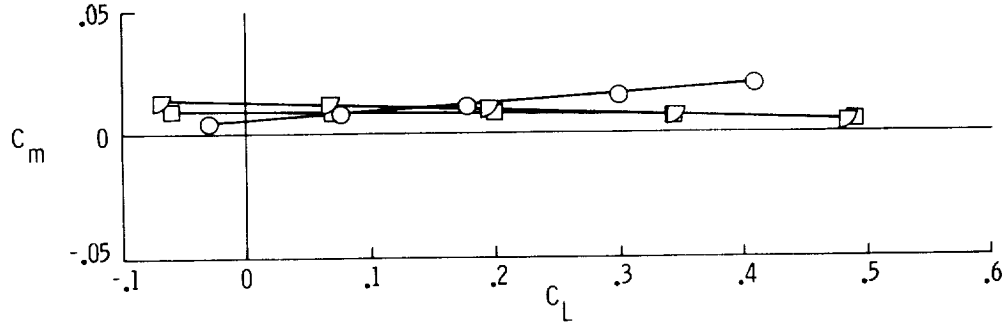

(b) −3° nacelle incidence.

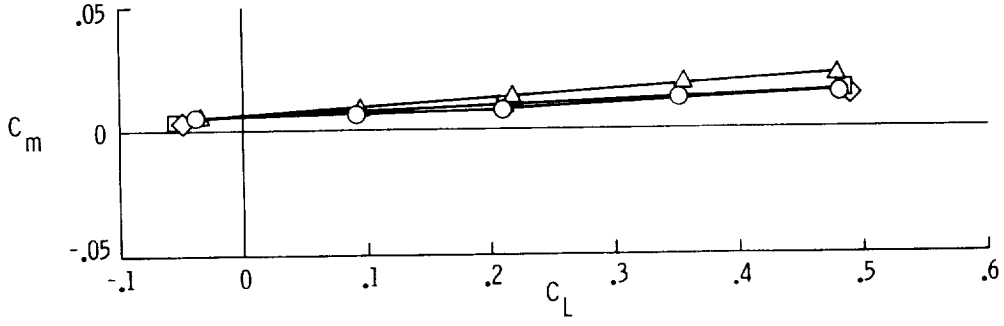

(c) 0° nacelle incidence with wing-tip extension.

Figure 12. Effect of nacelle and propeller installation on pitching-moment coefficient.

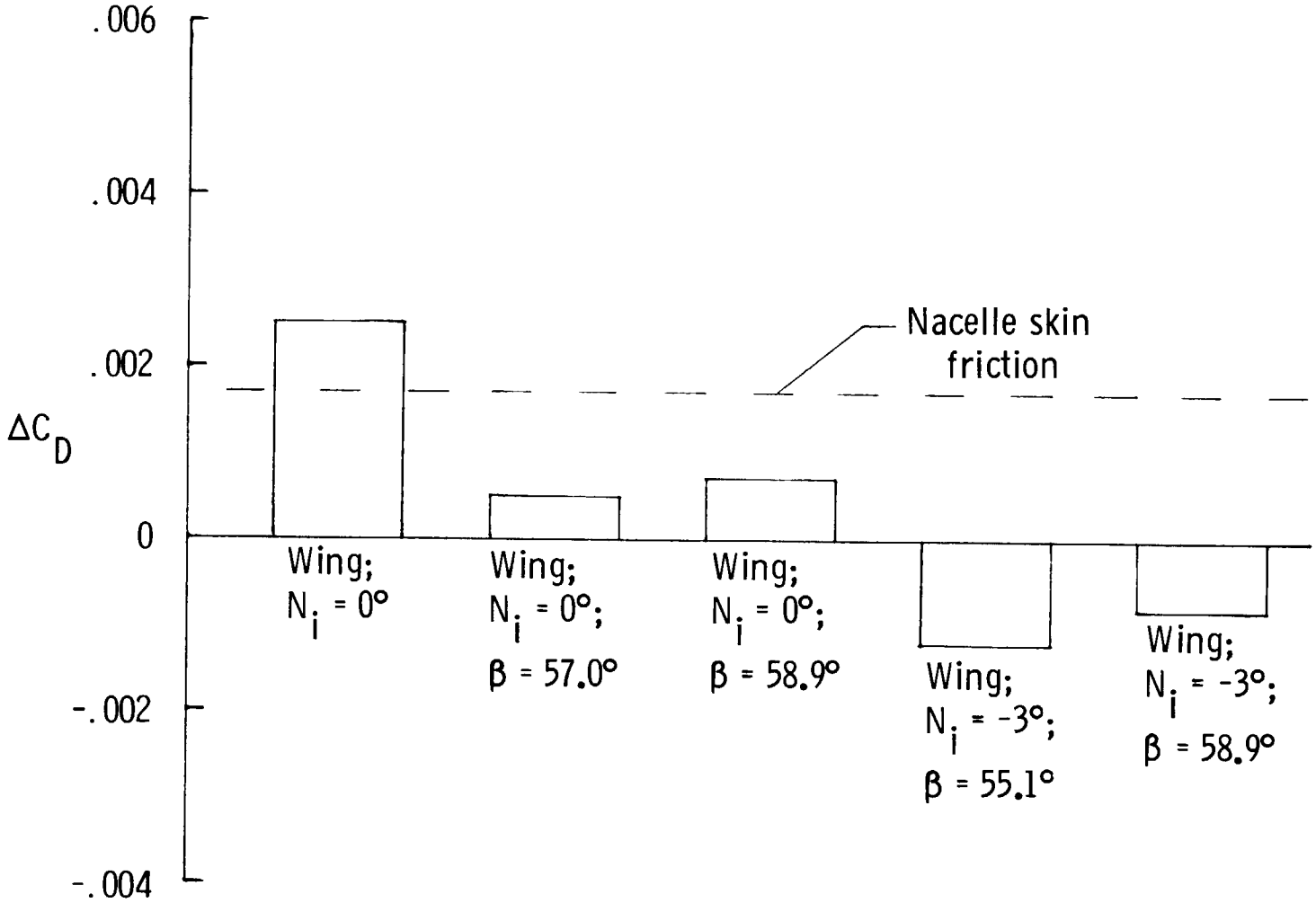

(a) Propeller rotation opposite vortex rotation.

Figure 13. Drag-coefficient increment from wing alone at $C_L = 0.3$.

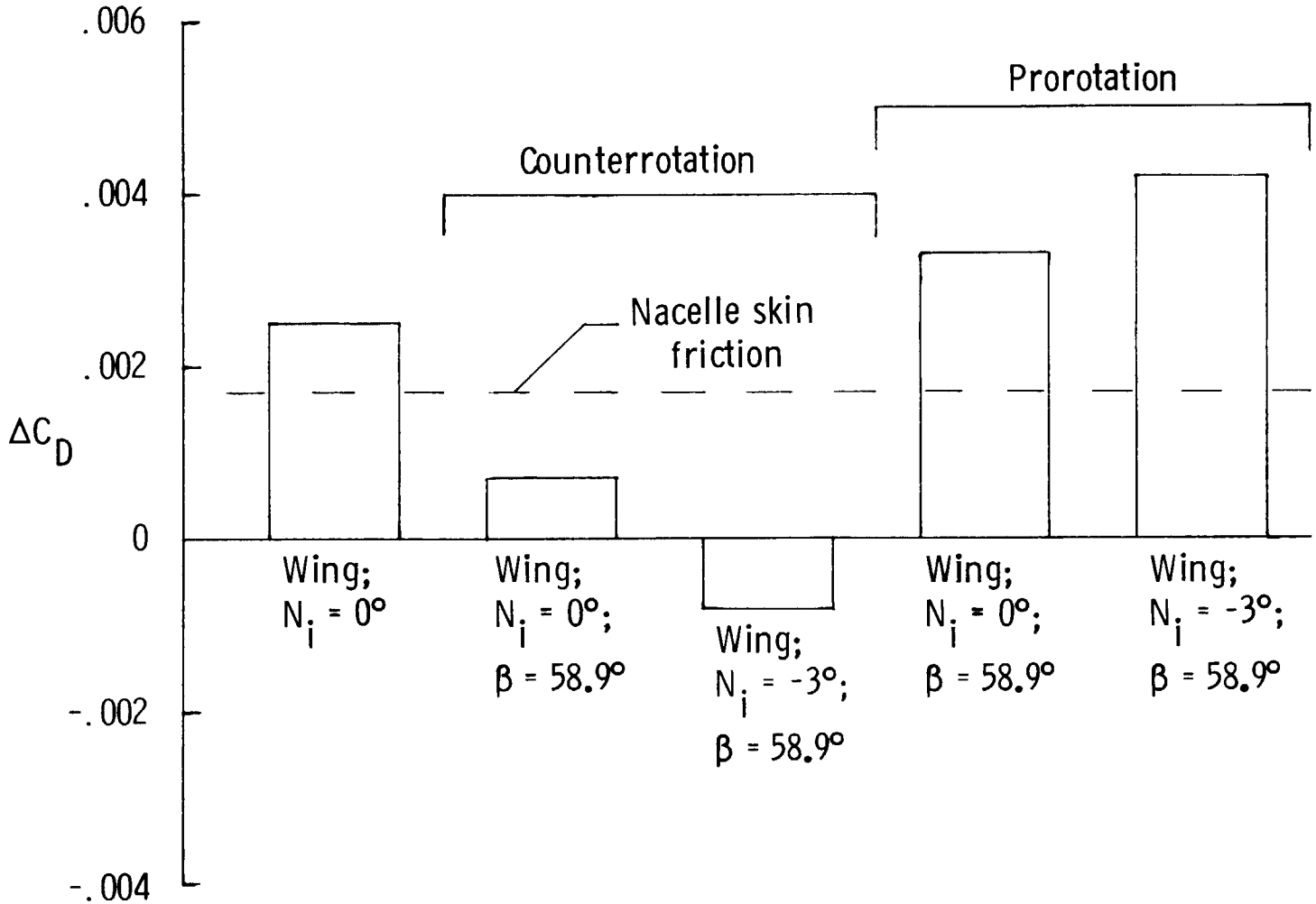

(b) Comparison of propeller rotation same as and opposite vortex rotation.

Figure 13. Continued.

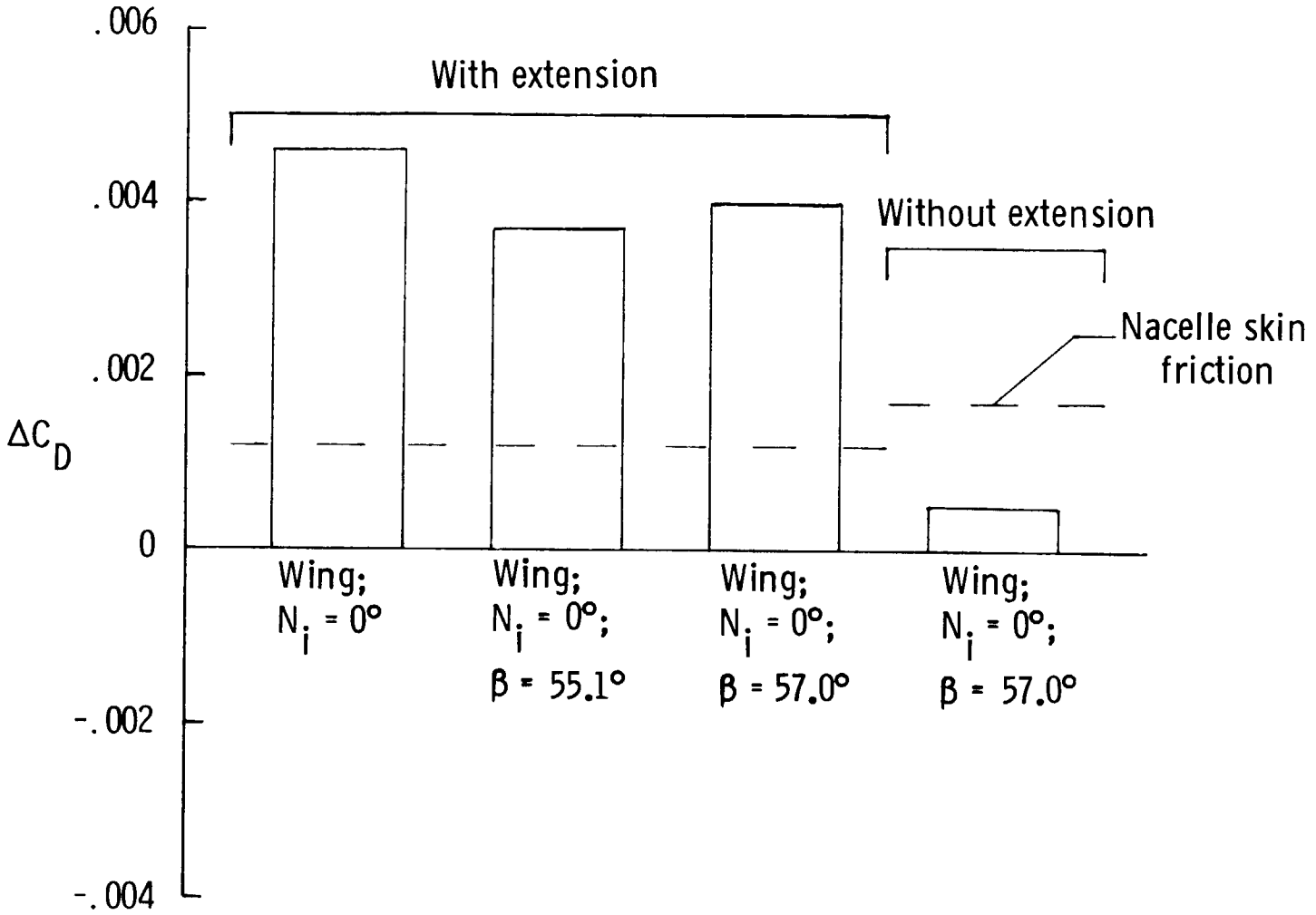

(c) Comparison with and without wing-tip extension for propeller rotation opposite vortex rotation.

Figure 13. Concluded.

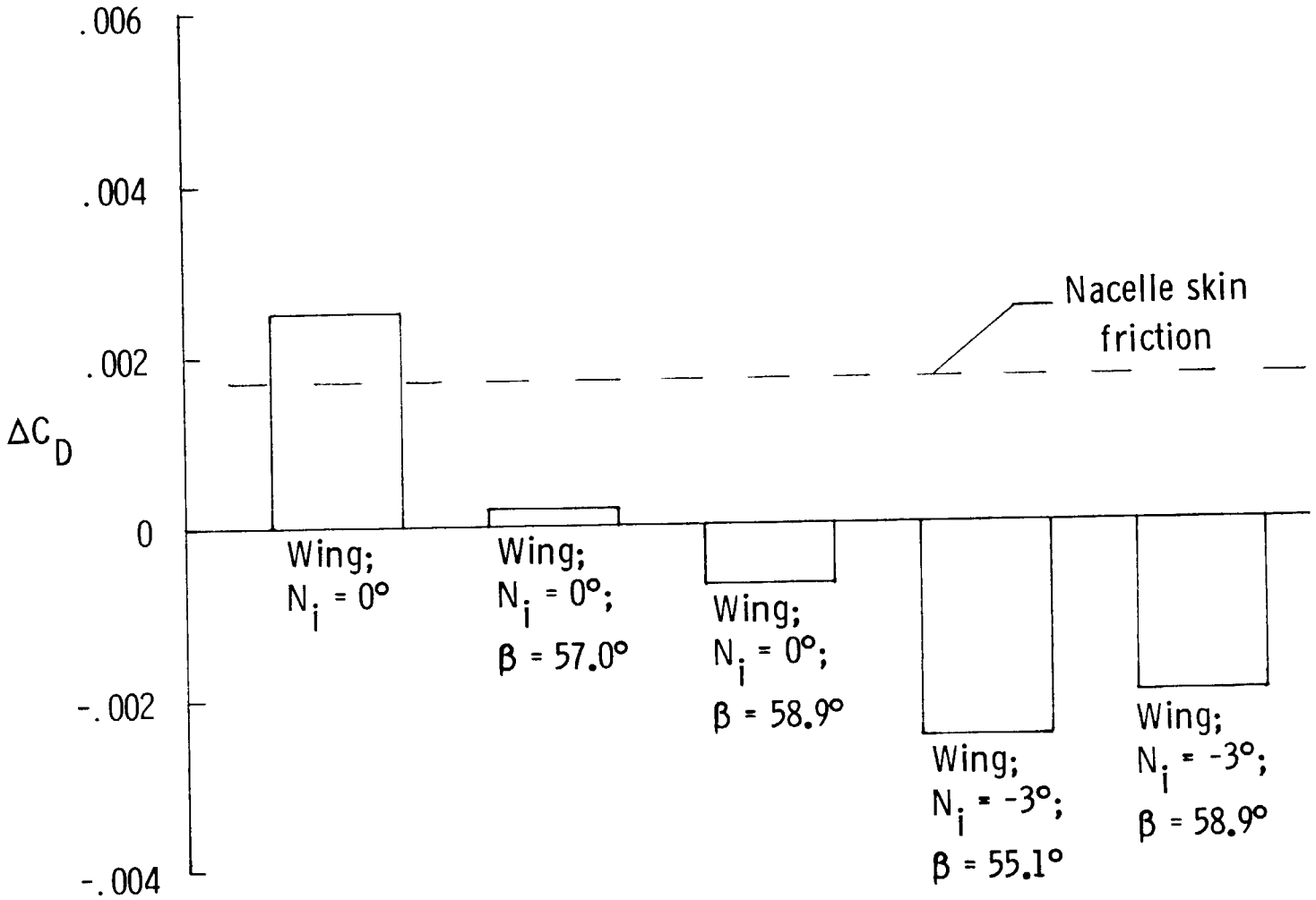

(a) Basic wing/nacelle/propeller.

Figure 14. Drag coefficient increment from wing alone at $C_L = 0.4$.

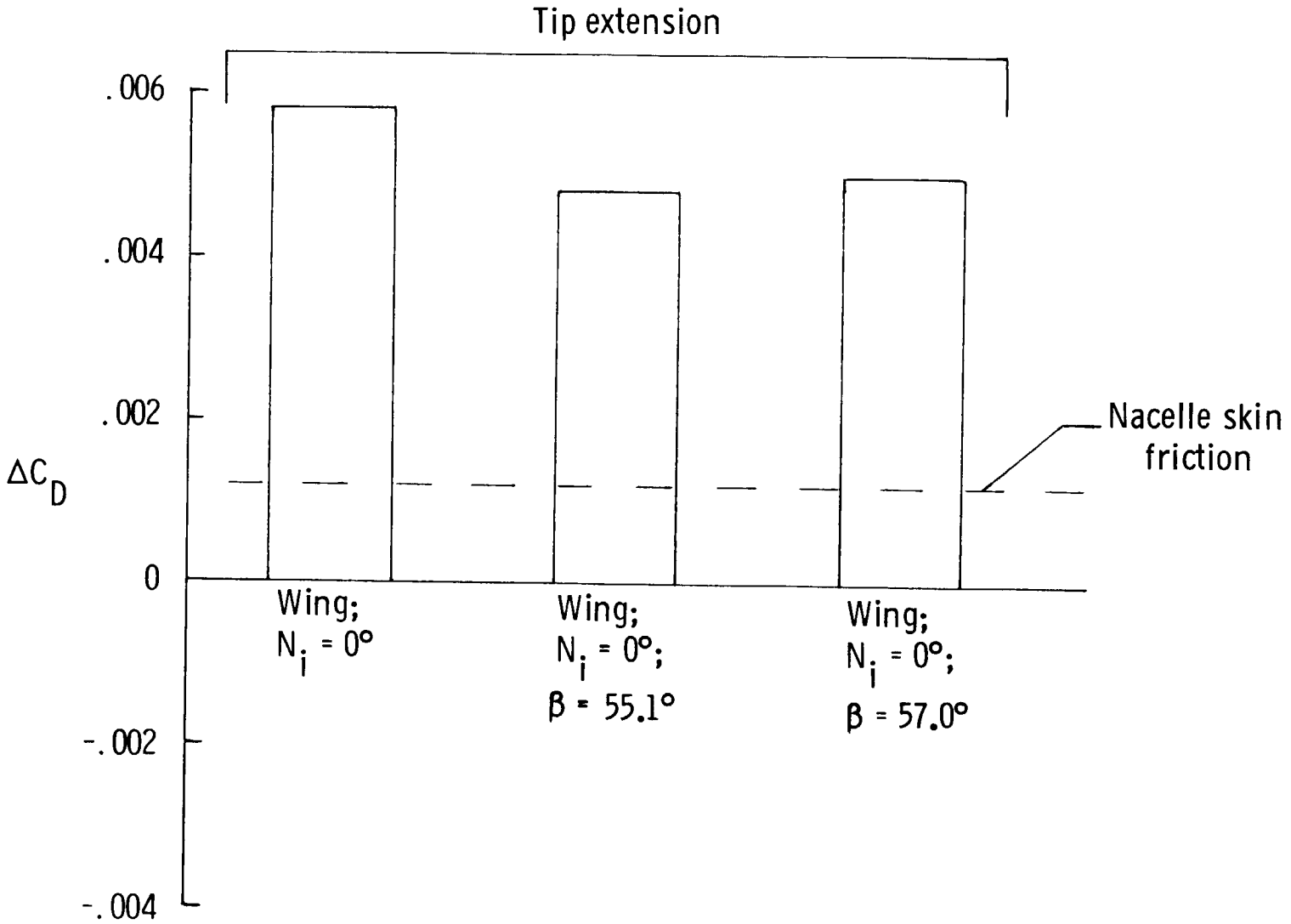

(b) Wing-tip extension.

Figure 14. Concluded.

NASA
National Aeronautics and Space Administration

Report Documentation Page

1. Report No.	2. Government Accession No.	3. Recipient's Catalog No.
NASA TP-2739		

4. Title and Subtitle	5. Report Date
Evaluation of Installed Performance of a Wing-Tip-Mounted Pusher Turboprop on a Semispan Wing	August 1987
	6. Performing Organization Code
7. Author(s)	8. Performing Organization Report No.
James C. Patterson, Jr., and Glynn R. Bartlett	L-16252
	10. Work Unit No.
9. Performing Organization Name and Address	535-03-01-01
NASA Langley Research Center Hampton, VA 23665-5225	11. Contract or Grant No.
	13. Type of Report and Period Covered
12. Sponsoring Agency Name and Address	Technical Paper
National Aeronautics and Space Administration Washington, DC 20546-0001	14. Sponsoring Agency Code

15. Supplementary Notes

16. Abstract

An exploratory investigation has been conducted at the Langley Research Center to determine the effect of a wing-tip-mounted pusher turboprop on the aerodynamic characteristics of a semispan wing. Tests were conducted on a semispan model with an unswept, untapered wing and an air-driven motor that powered an SR-2 high-speed propeller located on the tip of the wing as a pusher propeller. All tests were conducted at a Mach number of 0.70 over an angle-of-attack range from approximately $-2°$ to $4°$ at a Reynolds number of 3.82×10^6 based on the wing reference chord of 13 in. The data indicate that, as a result of locating the propeller behind the wing trailing edge at the wing tip in the crossflow of the wing-tip vortex, it is possible to improve propeller performance and simultaneously reduce the lift-induced drag.

17. Key Words (Suggested by Authors(s))	18. Distribution Statement
Turboprop Propfan Wing-tip vortex Wing-tip pusher propeller Vortex energy recovery Induced drag Performance Wing Propulsion Installation	Unclassified Unlimited Subject Category 05

19. Security Classif.(of this report)	20. Security Classif.(of this page)	21. No. of Pages	22. Price
Unclassified	Unclassified	28	A02

NASA FORM 1626 OCT 86

NASA-Langley, 1987

For sale by the National Technical Information Service, Springfield, Virginia 22161-2171